Design and Testing of NFRad—
A New Noise Measurement System

Chriss A. Grosvenor
James Randa
Robert L. Billinger

Radio-Frequency Technology Division
Electronics and Electrical Engineering Laboratory
National Institute of Standards and Technology
325 Broadway
Boulder, Colorado 80303-3328

March 2000

CONTENTS

Design and Testing of NFRad —
A New Noise Measurement System

Chriss A. Grosvenor
James Randa
Robert L. Billinger

Radio-Frequency Technology Division
Electronics and Electrical Engineering Laboratory
National Institute of Standards and Technology
Boulder, CO 80303-3328

The NIST Noise Project has constructed and tested a new, automated, coaxial (GPC-7) radiometer for the measurement of noise sources in the 8 GHz to12 GHz frequency band. It is an isolated, total-power radiometer that relies on lookup tables for relevant reflection coefficients and path asymmetry. Hence, much faster measurements at multiple frequencies result, compared to previous NIST systems. This technical note reviews the theory, describes the design of the system and its components, and details the testing procedures and the operation of the system.

Key Words: noise; noise figure; noise measurement; noise temperature; radiometer; thermal noise

1. INTRODUCTION

The National Institute of Standards and Technology (NIST) Noise Project has recently completed construction and testing of a new, automated, coaxial (GPC-7) radiometer for thermal noise measurements between 8 GHz and 12 GHz. The system was developed to measure noise figure, as well as noise temperature, and hence it is referred to as NFRad. Construction of similar radiometers for the bands 1 to 2 GHz, 2 to 4 GHz, 4 to 8 GHz, and 12 to 18 GHz is underway. Most of the present paper applies to all radiometers, though certain details are peculiar to the 8 to 12 GHz unit. These radiometers can also be used to measure waveguide devices through adapters.

NFRad represents the next generation of NIST radiometers. NFRad uses an isolated, total-power radiometer as in previous NIST systems [1, 2], but is now mechanically and electronically more stable so that it no longer needs to incorporate a six-port reflectometer for measuring reflection coefficients, mismatches, and asymmetries. Instead, reflection coefficients and asymmetries are measured using a vector network analyzer (VNA) and stored in lookup tables. This strategy allows us to make much faster noise measurements compared to previous radiometers, which relied on six-port reflectometers. We have added more ports to the switch

head, which increases the number of devices under test (DUTs) that can be simultaneously measured, thus increasing the speed of measurements. The increased speed and order-of-magnitude increase in stability are also essential for future noise parameter measurements. The six-port calibration and asymmetry measurement at a single frequency consumed about one half-day, whereas with NFRad that time can be dedicated to noise measurements. The previous NIST coaxial systems required about one full day for all measurements needed to calibrate a noise source at one frequency. The new system can make the same measurements at five frequencies in one half-day. No significant loss of accuracy is incurred in using a VNA rather than a six-port because VNAs now have accuracies comparable to those of six-ports. We rely on the fact that the relevant reflection coefficients, mismatches, and asymmetries are stable over time. Measurements will be repeated every few months to ensure that these system parameters remain unchanged.

This technical note reviews the theoretical background in Section 2 and describes the design and construction of the system in Section 3. Section 4 documents the system tests for the 8 to 12 GHz radiometer. The uncertainty analysis for this system is discussed in Section 5 and a brief summary is included in Section 6.

2. THEORETICAL BACKGROUND

The derivation of the radiometer equation depends on two assumptions. The first is that the radiometer responds linearly to the power delivered to it (the system has been designed to avoid power compression.) The second assumption is that the linear response of the radiometer does not depend on the source impedance, where sources include measured standards and DUTs.

2.1 General Noise Theory

To the extent that the system responds linearly to our signal, there are no higher order terms and the power spectral density at the output of our network is given by the power spectral density of the device at the input, multiplied by some transfer function of the network [3]. The power spectral density is the spectral power per unit bandwidth. Figure 1 shows a source, a detection system and a passive transfer network, designated by T_a. The transfer network generates its own noise power and adds this to the available power of the system so that,

$$P_{av(2)} = \alpha_{21}P_{av(1)} + \zeta P_a,$$

(1)

where α_{21} is the ratio of the available power at plane 2 to the available power at plane 1 in the absence of internal sources, and P_a is the noise power generated by the ambient network shown as α_{21}. The powers must conform to the condition that when all components are at an ambient temperature, then $P_{av(2)} = P_{av(1)} = P_a$. This requires that $\zeta = (1 - \alpha_{21})$ and thus,

$$P_{av(2)} = \alpha_{21}P_{av(1)} + (1 - \alpha_{21})P_a.$$

(2)

2

The delivered power at the radiometer is then given by the available power at plane 2 multiplied by a mismatch factor at plane 2 plus an effective input term that describes the power generated in the radiometer,

$$P_{del(2)} = M_2[\alpha_{21}P_{av(1)} + (1 - \alpha_{21})P_a] + P_{rad}. \tag{3}$$

2.2 Derivation of Radiometer Equation

Using the general theory given above, we can proceed toward the derivation of the radiometer equation. We will establish some notation and conventions before beginning with the derivation. Noise temperature is defined as the spectral density of available power from the source, divided by Boltzmann's constant k_B. Therefore, over a small bandwidth B in which the available power from the source is constant, the available power is given by $P = k_B B T_{noise}$. Available powers will be denoted by capital P and delivered power spectral density by a lowercase p. The subscript x will be used to denote the unknown DUT, the subscript s denotes the cryogenic standard and the subscript a denotes the ambient standard. The cryogenic standard [4] and the ambient standard are the primary NIST standards. The subscripts on the delivered powers and mismatch factors will indicate the reference plane and configuration. Thus $p_{2,x}$ refers to the delivered power spectral density at plane 2 when the switch has been switched to the DUT or unknown (x) port. The same notation holds for $M_{0,x}$, $M_{0,s}$, $M_{0,a}$, α_{03}, and α_{02} given below. The radiometer equation requires that two delivered powers be known to determine the noise temperature of an unknown device. The equations are based on the previous subsection and the diagram shown in Figure 2. We will follow the derivation given in references [1] and [2]. Our
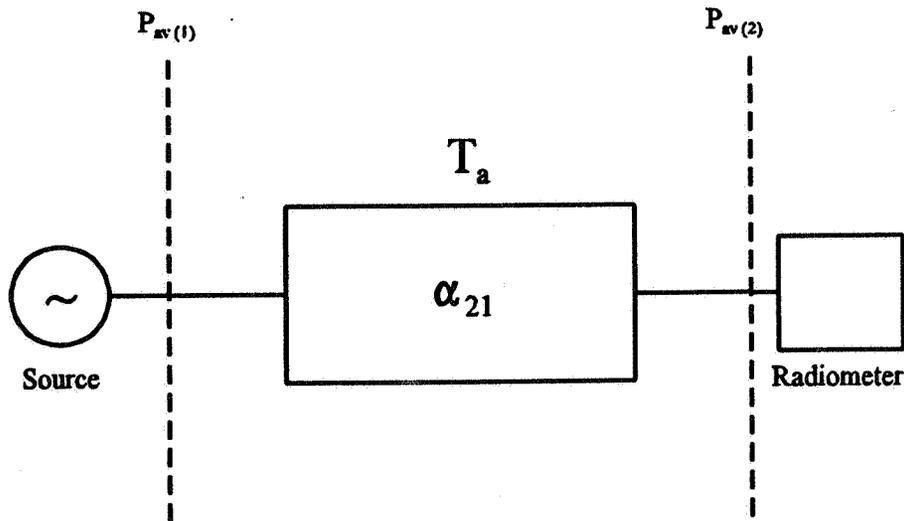

Figure 1. General theoretical development.

3

three measurement equations are given by

$$p_{0,x} = M_{0,x}[\alpha_{03}T_x + (1 - \alpha_{03})T_a] + p_{ex},$$
$$p_{0,s} = M_{0,s}[\alpha_{02}T_s + (1 - \alpha_{02})T_a] + p_{es}, \tag{4}$$
$$p_{0,a} = M_{0,a}T_a + p_{ea},$$

where a factor of $k_B B$ is understood to multiply the noise temperatures. If we combine these equations and define the ratios $\dfrac{p_{0,x}}{p_{0,a}} = Y_x$ and $\dfrac{p_{0,s}}{p_{0,a}} = Y_s$, we obtain the following radiometer equation,

$$T_x = T_a + (T_s - T_a)\frac{(Y_x - 1)M_s\eta_s}{(Y_s - 1)M_x\eta_x}, \tag{5}$$

where we have used $M_{0,x}\alpha_{03} = M_x\eta_x$ and $M_{0,s}\alpha_{02} = M_s\eta_s$. The quantities M_s and M_x are the mismatch factors at planes 2 and 3, respectively, η_s is the efficiency or ratio of delivered power between planes 0 and 2, η_x is the efficiency or ratio of delivered power between planes 0 and 3. M_x and M_s are given by the following expressions,

$$M_x = \frac{(1 - |\Gamma_x|^2)(1 - |\Gamma_{3,r}|^2)}{|1 - \Gamma_x\Gamma_{3,r}|^2},$$

$$M_s = \frac{(1 - |\Gamma_s|^2)(1 - |\Gamma_{2,r}|^2)}{|1 - \Gamma_s\Gamma_{2,r}|^2}, \tag{6}$$

There is another term, not shown, which contributes to the isolation and connector errors discussed in the uncertainty section. The mismatch factors are determined from the reflection coefficients of each device or standard Γ_x, Γ_s looking back through the switch path toward the radiometer $\Gamma_{2,x}$, $\Gamma_{2,s}$, where again the reflection coefficients are no longer measured with an internal six-port but are measured on a VNA. The efficiencies are no longer measured as asymmetries between the measurement ports [1, 2], but are directly measured using the VNA. This is discussed below.

3. DESIGN/CONSTRUCTION AND OPERATION

3.1 Overview

The system measures the noise power from the various standards and the DUT. The
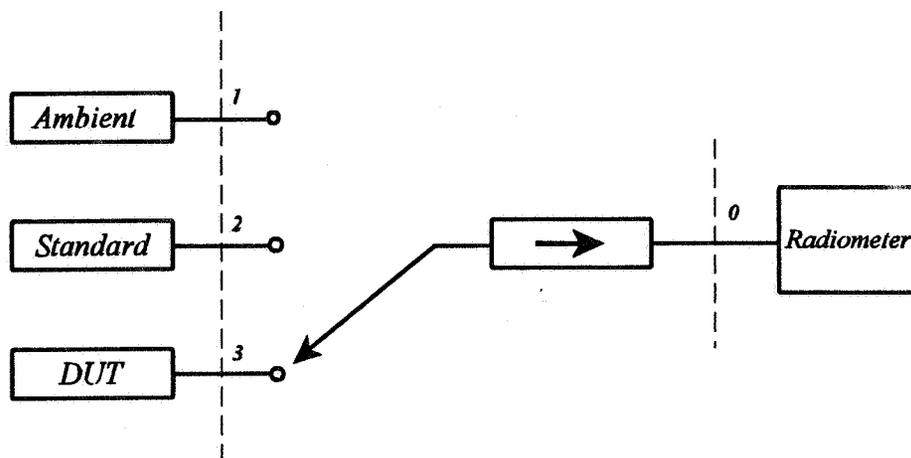
Figure 2. Basic setup for measurement of noise temperature.

measured powers are then used to calculate the noise temperature of the DUT. The power from each DUT is of the order of 10^{-12} W in our 5 MHz measurement bandwidth. Because there are no detectors currently available to measure these low powers, the signal is amplified and refined in various stages until it can be measured by a thermistor. The whole system has about 100 dB of gain.

The current design of NFRad is an improvement on earlier waveguide and coaxial systems. The design focus for this system was on stability and increased speed for noise temperature measurements. The increased speed also makes it more practical to measure the noise parameters of amplifiers. A photograph of the system is shown in Figure 3. From top to bottom, the test equipment is as follows: a digital multimeter, a synthesizer, two switch-control units, a circuitry section, a unit housing power supplies, and the IF section.

A block diagram of the system is shown in Figure 4. The following subsections discuss the function of each element in the block diagram. The radio-frequency (RF) and intermediate-frequency (IF) sections are composed of several microwave components; however, for diagram simplicity only the major components are shown. As these two sections are discussed, a detailed block diagram will be shown. The connections to power supplies, switches and various other circuitry are not shown but will be discussed below.

3.2 Switch Head Assembly

The switch head assembly is the first major element in the system block diagram. The switch head has six measurement ports and one common port. The radiometer is attached to the common port, and the primary standards, check standards, and DUTs are connected to the other ports. This allows us to conveniently switch between ports without disconnecting any device. A photograph of this assembly is shown in Figure 5. The first port is reserved for the
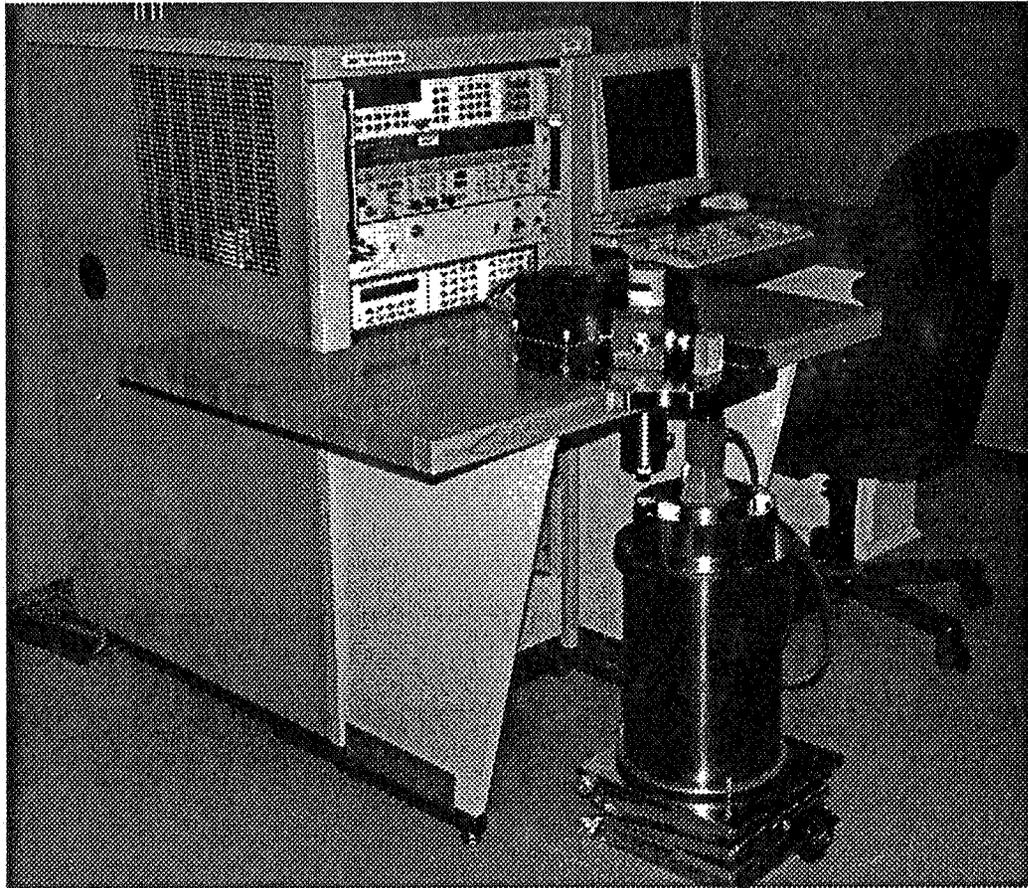
5

Figure 3. Measurement equipment used for noise-temperature measurements.

ambient standard and is located internal to the housing. Port 2 is on the bottom of the assembly and is reserved for the cryogenic standard, which must remain vertical when filled with liquid nitrogen.

The important design concepts for the switch head were temperature stability and mechanical rigidity. Temperature stability is maintained using a series of water channels throughout the assembly. The assembly is made of stainless steel. Using this material allows us to maintain temperature equilibrium and mechanical rigidity. Because S-parameters and reflection coefficients are no longer measured for every device, the rigidity of the structure ensures that the S-parameters of the switch head remain constant.

3.3 Radiometer/RF Section

A photograph of the 8 to 12 GHz radiometer is shown in Figure 6. Inside the radiometer structure is the RF section and a thermistor, both of which are mounted on a water plate. As the RF signal enters the radiometer it passes through a 40 dB isolator (see Figure 7). After this point, the signal can be switched either to an outside port to measure the S-parameters of the isolator or
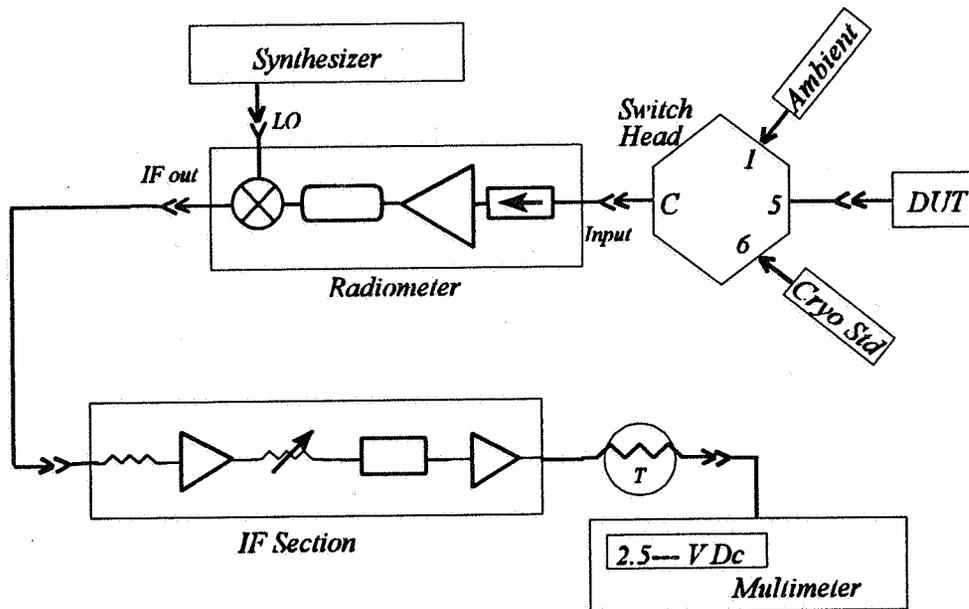
6

Figure 4. System block diagram

Figure 5. A 8 to 12 GHz radiometer.

7

into the RF section. In the RF section, the signal passes through a second 20 dB isolator. The combined isolation minimizes the dependence of the radiometer output on the source impedance. After the isolators, the signal is amplified and then filtered using a 12.4 GHz low-pass filter. The RF amplifier generates heat and so the water plate is used to maintain an ambient temperature within this structure.

In the final stage the RF signal mixes with a local-oscillator (LO) signal from the synthesizer using a double-balanced mixer. Incorporated in this system is an automatic level-control (ALC) circuit that ensures that the LO power into the mixer is constant. After mixing, the IF signal is fed into the IF section. There is a second set of similar circuits located in the same box to control a separate but identical radiometer. These two circuits are designated Channels A and B, respectively.

3.4 IF Section

A schematic of the IF section is given in Figure 8. The IF section is the final stage of amplification before the output signal is measured at the thermistor. In this section, the IF linearity test is performed and the system gain is controlled. The first component in this section is a 3 dB attenuator, which is used to check the IF linearity of the system. This test is discussed in section 4. The signal is then passed through the first IF amplifier. The next attenuator is a variable 127 dB latching attenuator, which is used to control the gain. Most diodes that we measure generate noise at around 9000 K, which requires an attenuator setting of 6 dB for an output signal

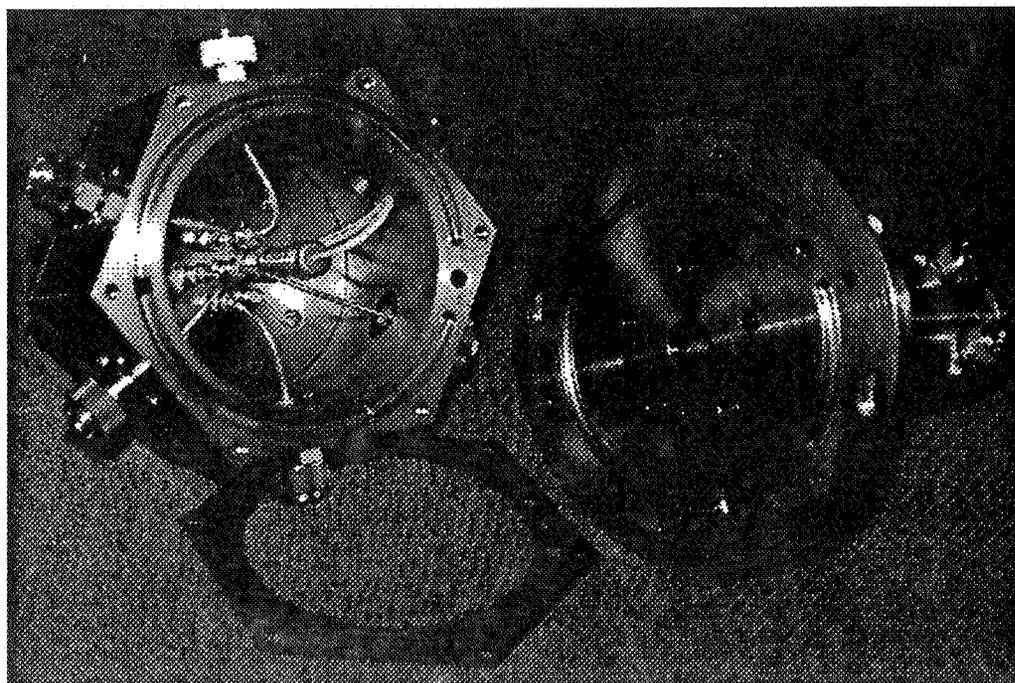Figure 6. The interior of the switch head assembly. The copper tube in the center houses the thermistor and the 50 Ω coaxial load.
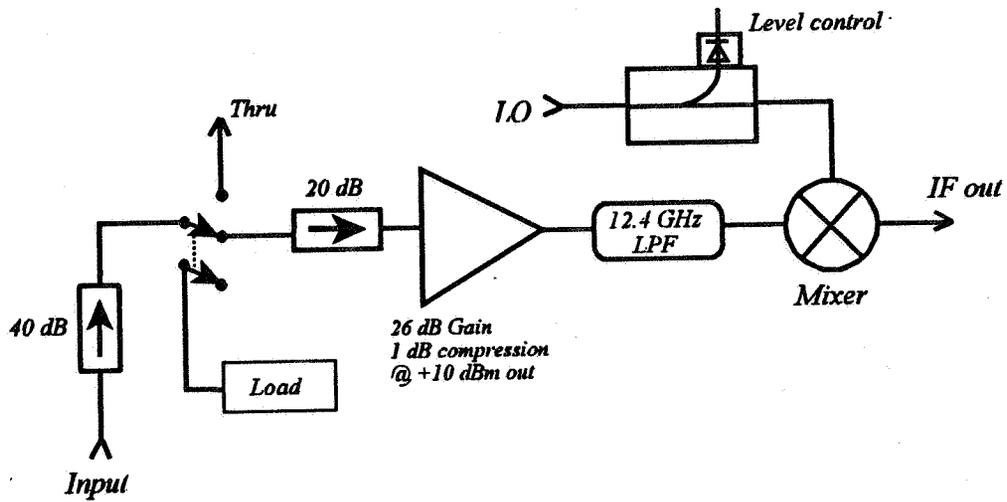
8

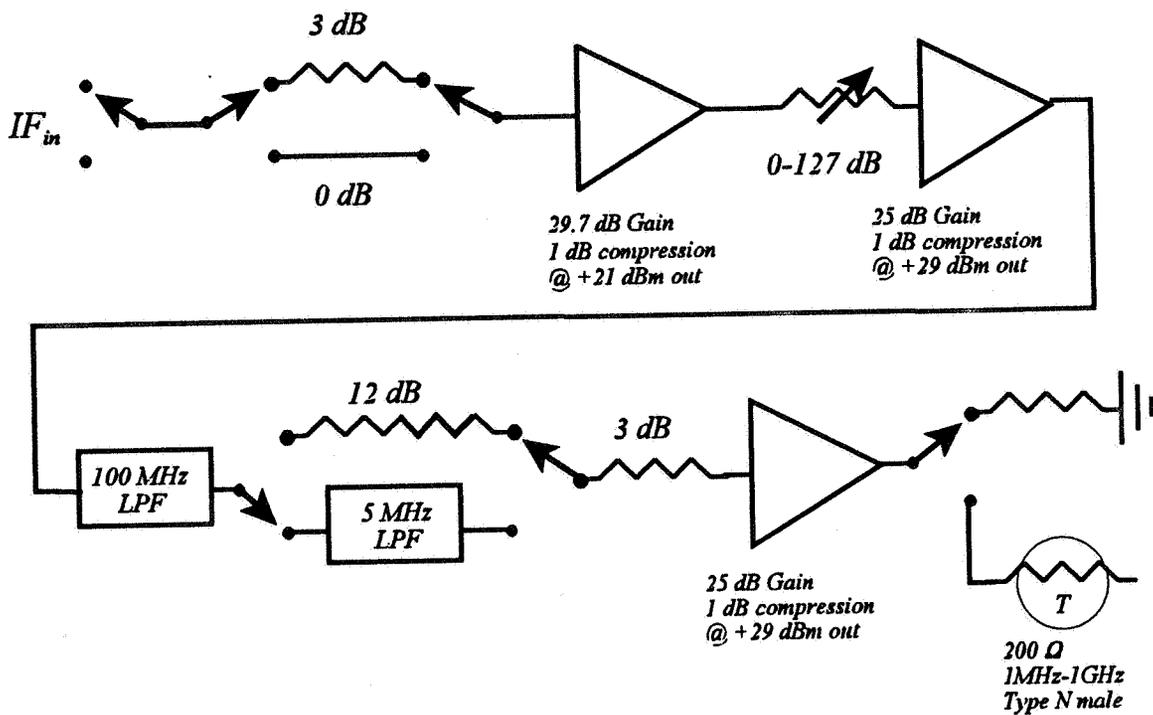Figure 7. RF section for noise-figure radiometer system.

Figure 8. IF Section for noise-figure radiometer system.

level between 5 and 6 mW. This is a midrange number for the IF section and falls well within our critical output levels from 0.01 mW and 10 mW. This linear region will be shown during the testing section of this report. The entire IF section is also mounted on a water plate to maintain a constant ambient temperature. After passing through the attenuator, the signal is again amplified and then passed through a 5 MHz, low-pass filter. The filter determines the IF bandwidth of the system. The other optional bandwidth is 100 MHz. The final stage in this section is a 3 dB attenuator and a 25 dB gain amplifier. The signal should now be within the measuring range of the thermistor. The bandwidth of the thermistor is 1 MHz to 1 GHz. Since our signal bandwidth is <5 MHz, the thermistor measures the noise over a 1 to 5 MHz bandwidth. There are two reasons why we do not want to measure signal noise below 1 MHz. The first is that commercial thermistors have a DC blocking capacitor that introduces nonlinearity below about 1 MHz. The second reason is that other types of noise (e.g., flicker or 1/f) dominate at lower frequencies.

At this point, the multimeter is used to measure the voltages from the thermistor using a NIST Type IV power meter card [5]. These voltages are converted to power using a DC-power substitution method [5]. The multimeter is also used to measure the 28 V dc bias for diode DUTs and check standards.

3.5 Switch/Control Units

There are two switch/control units used in the system to control the switching between various circuits. Both have a total of five cards available. The first switch/control unit uses all five cards; and the second uses three cards. In Card 1 of the first unit, 24 V is tied to the solenoids on channels 00 through 04 (delay circuits-channel A) and 24 V is tied to the solenoids on channels 05 through 09 (ambient circuits-channel A). Card 2 is set up the same way, except it controls the ambient and delay circuits for channel B. There is one delay or ambient circuit tied to each channel. When a particular channel is selected, the high or low side of the common bus is grounded, thus completing the circuit for that particular channel, and the switch is thrown. The switch must be closed and then opened, otherwise the circuit will heat up and add unwanted heat to the system. In unit 1, card 3 controls the selection of all 24 V power supplies. Cards 4 and 5, channels 00 through 05 select various thermistors for measuring temperature. Channel 08 is used to read from the Type-IV power meter card, and channel 09 is used for the reference voltage generator. In switch/control unit 2 there are three cards used (1, 2, and 5). Card 1, channels 00 through 06, selects attenuation for the variable 127 dB attenuator in the IF section. Channels 07, 08, and 09 are used to select either channel A or B, or the 5 MHz or 100 MHz filter, or to turn the RF on or off. Card 2 selects or deselects the first 3 dB attenuator in the IF section. On Card 5, channels 08 and 09 are attached to the power supply relay to select 12 V for either the high or low side of the card. Channel 00 (high side) and channel 01 (low side) are the 24 V returns, and channel 02 (high side) and channel 03 (low side) are the 12 V supply for selecting and deselecting the IF attenuation.

We will illustrate how the cards switch from any port on the switch head to port 1. Figure 9 diagrams the terminal block for the power supplies. The wiring configurations for Card 3 in Switch/Control Unit 1 and for Card 5 in Switch/Control Unit 2 are shown in Figure 10. To switch

10

from any port to port 1, the first command given to the system is "OPEN 500." On card 5, channel 00, the switch is opened to disable the ground on the low side.

The next command is "CLOSE 501." On card 5, channel 01 closes the switch to enable the ground on the high side. The next command, "CLOSE 509," grounds pin 14 in Figure 9. Because pin 17 already has a positive voltage on it, the circuit is completed and the relay switch on pins 15 and 18 are thrown. This puts 24 Vdc at the switch head (this voltage is needed to throw the mechanical, coaxial switches). The switch is toggled using the next two commands, "CLOSE 304" and "OPEN 304." When we close channel 04 on card 3, the high side of the card is grounded, which completes the circuit at port 1, thus supplying current to the solenoid that closes the mechanical switch. Port 2 is also operated using channel 04, card 3, but is activated when ground is applied to the low side of the card. All ports not chosen are terminated in 50 Ω. The port that is chosen is tied to common and will not be terminated in 50 Ω.

3.6 Operation

To begin a noise-temperature measurement the following procedure is used. The radiometer is connected to the common port, which is inscribed with the letter C. The 7 mm cryogenic standard is charged (filled with liquid nitrogen to a predetermined level) and connected
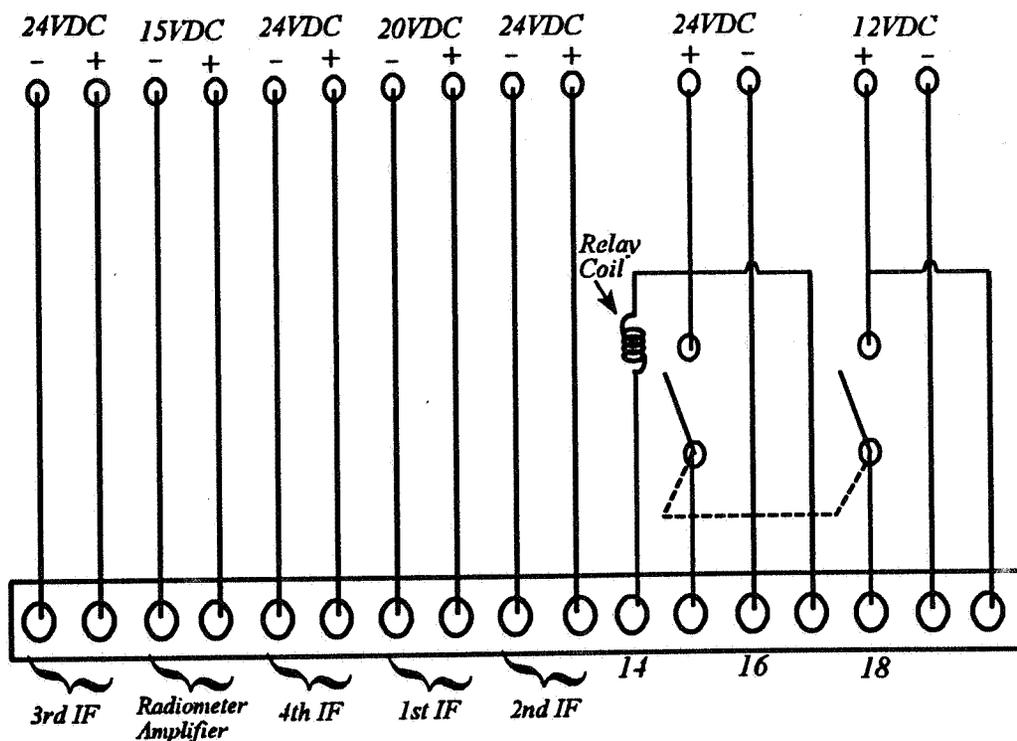

Figure 9. Power supply rear panel terminal block.

11

to port 2, which is under the table (see Figure 3). The system is left in a power-on state so that equipment reaches and maintains equilibrium conditions. The power supply is turned down, not off, after every measurement; therefore the diodes that we measure are not pulsed with RF, but are gradually turned on. The power supply for the diodes is set to 28 V before we begin measurements. The software program's initial screen shows the default values set for each instrument and measurement. These can be changed in the program but are initially set as discussed in what follows. The system measures the standards and DUT a total of 25 times for a 3 dB attenuator switched into the circuit and 25 times for the 3 dB attenuator switched out of the circuit. In our current measurement scheme, the Type-IV power-off measurement (no IF supplied to card) is taken first, the ambient standard second, the cryogenic standard third, the check standard fourth, and the DUT fifth; and then the ambient standard is measured again. The ambient standard is assigned to port 1 (this is its permanent physical location), the 7 mm cryogenic standard is assigned to port 2, the default location for the check standard is port 5, and the default location
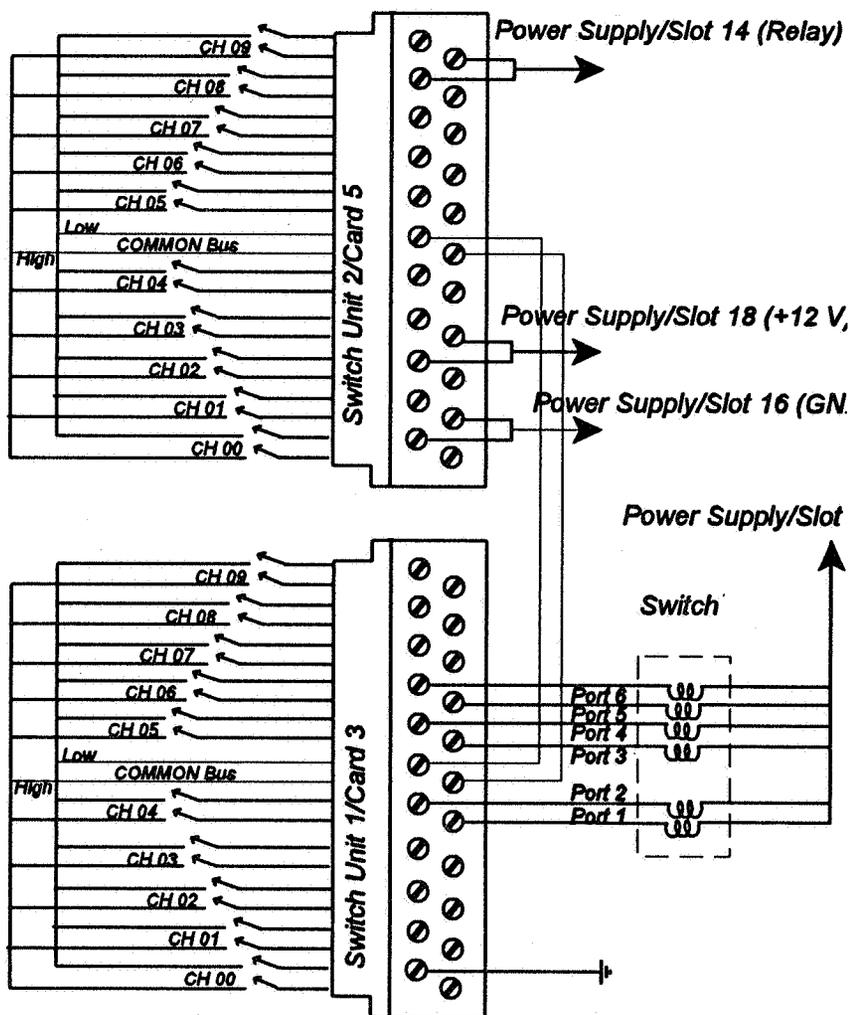

Figure 10. Switch/control card wiring for card 3 and card 5.

for the DUT is port 6.

The first procedure in the software, after defining or redefining default values, is to initialize all instrumentation to its default state. S-parameters or reflection coefficient files are then read for each device and for the switch plus radiometer combination. The program then turns the IF off, switches to either channel A or B, selects the 5 MHz filter and selects 6 dB of attenuation for the variable 127 dB attenuator in the IF section. The 3 dB attenuator is switched out of the circuit for the first 25 measurements. The RF is turned on at the synthesizer, and the first frequency is set. The second step is to read the ambient temperature thermistors and calculate the temperature in kelvins for each one. There are a total of three thermistors in the system. One is located in the ambient standard in the switch head, one is in contact with the ambient load in the radiometer, and one is in the water line path just before the water enters the cryogenic standard's neck. The third step is to read the atmospheric pressure (in mm Hg) from the laboratory barometer and input this into the program, which calculates the boiling temperature of the liquid nitrogen in the cryogenic standard. At this point, the program begins taking power readings for each of the noise sources (primary standards, DUTs, and check standards). Actually, voltages are read from each device and are then converted to powers using the DC substitution equation,

$$P(mW) = \frac{(V_{off}^2 - V_{on}^2)}{2*R} * 1000 , \tag{7}$$

where R is the resistance of the thermistor, V_{off} is the Type-IV power-off reading, and V_{on} is the measured voltage of the device. The powers are measured by the Type IV power meter card after being amplified in the radiometer and IF sections. The ambient temperature is measured in the switch head, and the cryogenic temperature is calculated from the boiling point of liquid nitrogen for the atmospheric pressure measured in the lab. These will be discussed in the following sections. After 25 measurements, the 3 dB attenuator is switched into the circuit and another 25 measurements are taken. We require that the averages of these two sets of 25 measurements differ by no more than 0.2 %. The program computes the average temperature and standard deviation for each device. These are then fed into another routine to determine the Type-A and Type-B uncertainties (see Section 4) for the complete measurement. A file showing all powers and temperatures measured or calculated during the 50 measurements is printed. It also shows the average power for each 3 dB attenuation setting and the average temperature and its standard deviation. Another file is generated that contains all pertinent reflection coefficients, temperatures, mismatch factors, and efficiencies so that the measurement can be replicated.

4. TESTING

4.1 General Strategy

Before using the system for everyday measurements, several tests must be performed to verify that the system is operating correctly. We test the two assumptions made in deriving the radiometer equation; namely, the linearity and the isolation. We must test the values calculated

from the primary standards, and the values of the mismatch factors and path asymmetries measured by the VNA. We also must make sure that the signal we are measuring is the signal from the DUT and not some unwanted signal. Each test is described in the subsections below. A simple block diagram of the entire system is shown in Figure 11.

4.2 Cryogenic Standard

The first quantity to be discussed is T_n, the noise temperature of the cryogenic standard. The boil-off temperature of liquid nitrogen is a very well known quantity. The boil-off temperature of liquid nitrogen at various barometric pressures is given in Table 3, page 10 of reference [4]. The liquid nitrogen boils off inside the Dewar whose design is detailed in reference [4]. The physical temperature of the surface of the liquid nitrogen is computed from the boiling point at the atmospheric pressure in the lab. The load inside the Dewar is submersed in liquid nitrogen and is assumed to be at the temperature of the surrounding liquid nitrogen. The temperature at the depth of the load is calculated using the equation of state of liquid nitrogen. To obtain the noise temperature of the load from its physical temperature, we can use the following equation,

$$k_B T_{noise} = \frac{hf}{e^{\frac{hf}{k_B T_{phys}}} - 1} ,$$

(8)

where h is Planck's constant, f is the frequency, and k_B is Boltzmann's constant. With certain hot devices or at lower frequencies we use the assumption,

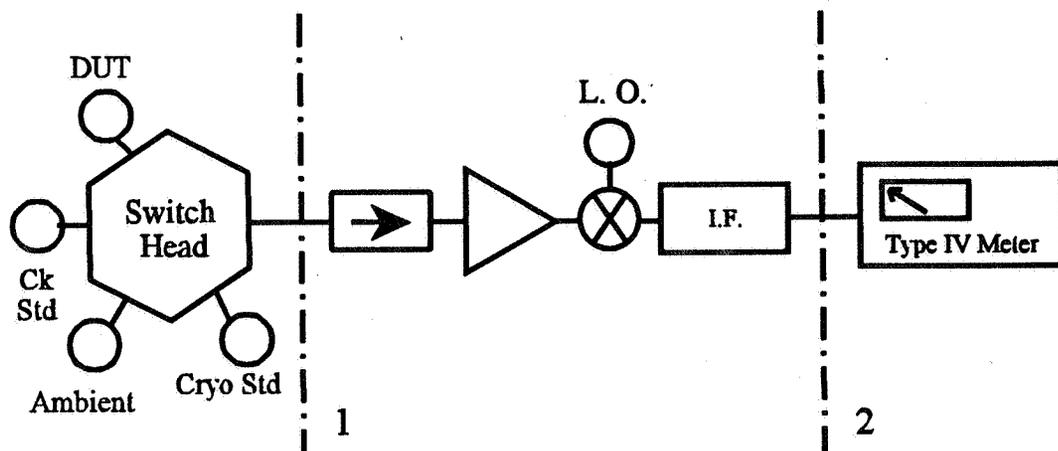$$\frac{hf}{k_B T_{phys}} \ll 1 ,$$

(9)

Figure 11. Block diagram of noise-figure radiometer system.

14

so that the physical temperature T_{phys} is approximately equal to the noise temperature. Finally, to determine the noise temperature at the output port of the cryogenic standard, corrections are made to account for various losses in the coaxial line.

The cryogenic standard has been in use for many years. The only new element is new software for computing the noise temperature at the output for a given atmospheric pressure. To test this section of the software we compared the boiling temperature computed in the new software to that found in reference [4]. The computed output noise temperature was then compared to the calculated output noise temperature in a completely independent module written by a different programmer in a different language.

4.3 Ambient Standard

The ambient temperature T_a is the noise temperature of the ambient standard. In our system, we have a coaxial load that is maintained at a temperature near room temperature, around 296 K. A thermistor measures the exact temperature. This physical temperature is then converted to a noise temperature using eq (8). The power from the load is measured to obtain the ambient output power. The thermistor and load are located inside the switch assembly and will be discussed later. Two other thermistors track the ambient temperature throughout the system. One is located inside the radiometer housing and the other is placed in the water line just before the cryogenic standard. All thermistors are calibrated at an outside lab, and a resistance value R1 at temperature T1 is supplied as well as another value of resistance R2 at temperature T2. These values are then inserted into the following equation to give us a calculated temperature in Celsius,

$$T_{celsius} = \frac{T2-T1}{R1-R2} (R1 - Meas) + T1 , \qquad (10)$$

where *Meas* is the measured four-wire resistance of the thermistor.

4.4 Stability

It is important to know the stability of the radiometer during a measurement of a customer's device. To measure the stability of the radiometer, we track the power and temperature of the ambient standard over a certain period of time. For the most recent test we measured the ambient standard over a 15 h period. In comparison, a typical customer measurement would take approximately 6 h for 5 frequencies and 50 independent measurements. For each independent measurement, we measure the ambient standard, the cryogenic standard, the check standard and the DUT, and then the ambient standard. During this series, the ambient standard must remain stable.

The results of this test are shown in Figure 12. For each measurement or data point on the plot, the ambient was read 100 times. Between every two measurements there is a delay of 5 min. This sequence is repeated until the end of the set time period. A linear fit was imposed on the data and the following characteristics were obtained. The slope was 8.639×10^{-6} mW per hour and the

15

y-intercept was 0.79911 mW. The slope shows that the measurement drifted no more than 0.001 % per hour.

It is useful to understand the construction of the switch-head ambient standard, and how we are able to maintain the temperature stability. A port on the coaxial switch was selected as the ambient port. Once the port was chosen, a port-size hole was drilled into a copper tube cap and slipped over this port (see Figure 13). A 50 Ω coaxial load was then connected to the port, and a short piece of copper tubing was added along with another cap. A small hole was drilled through the cap and a four-wire ohm thermistor and thermal paste were inserted into the entire assembly. The coaxial switch was then connected into the switch housing. During a measurement, the switch housing is maintained at room temperature by a series of channels designed to circulate water. To measure the temperature of the ambient, a four-wire resistance measurement is made, from which the temperature of the ambient is calculated. The ambient standard thus consists of a coaxial load and a thermistor to measure its temperature, in a cylindrical copper tube that is filled with thermal paste.
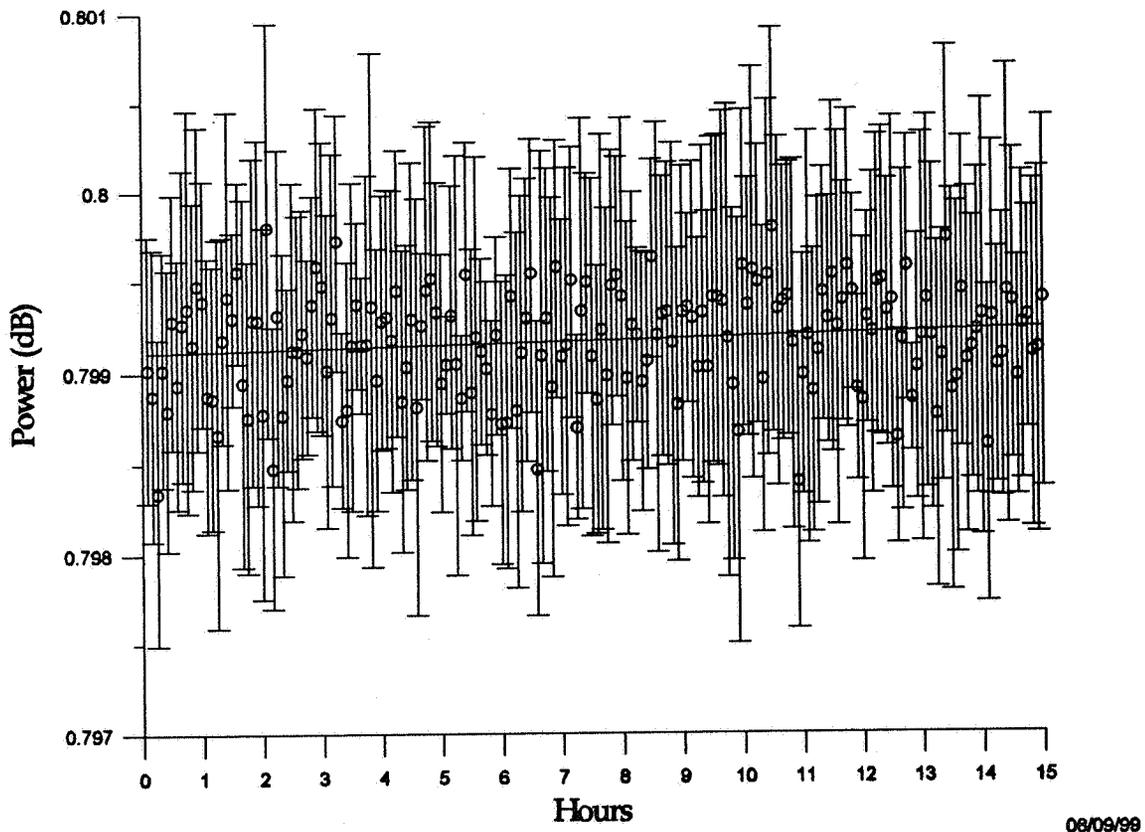

Figure 12. 8 GHz to 12 GHz radiometer stability test. Circles represent the measured values and the bars represent computed standard deviations for that measurement.
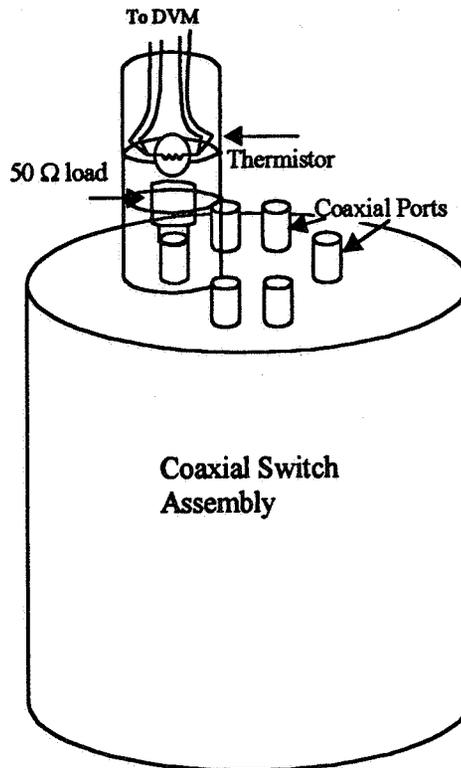
16

Figure 13. Construction of switch ambient housing.

4.5 Isolation

One of the assumptions we made in deriving eq (5) was that the output from the radiometer is independent of the noise source impedance. In the construction of the radiometer, two isolators are inserted at the input of the radiometer to isolate the radiometer from the source. To test this isolation, we measured the value of the two isolators at the input to the radiometer using a VNA. Since isolators are band-limited, we measured the isolators from 8 to12 GHz. The first isolator is specified to provide 40 dB of isolation and the second 20 dB of isolation, for a total input isolation of approximately 60 dB. The measurements showed that the first isolator provides approximately 42 dB of isolation across the frequency band, and the second provides approximately 21 dB across the band. Together, the two isolators provide greater than 60 dB of isolation across the band.

4.6 Linearity

The other assumption behind eq (5) is that the system responds linearly to the input powers from each device across the frequency band of interest. There are three potential sources of nonlinearity; the most likely source is in the IF section. The powers entering the IF section have already been amplified, and further amplification of the signal could drive the amplifiers into the nonlinear region. The other two potential sources of nonlinearity are the RF section and the mixer.

17

The mixer linearity test ensures that a small change in the LO power does not appreciably effect the measured temperature. The test procedure is as follows. The noise temperature of the standards is measured for an output synthesizer power of 10 dBm. The output power of the synthesizer is decreased by approximately 3 dBm and the noise temperatures are measured again. These should agree to within 2σ. At 9 GHz, check standard X12ZHZ.565 measured 9681 ± 17 K for the first measurement and 9687 ± 17 K for the second measurement. Since the difference between the measurements is less than 2σ, we conclude that the mixer is operating linearly.

The IF linearity test determines the linear operating range of the IF section for various output powers. The IF linearity test was conducted as follows. In the IF section, Figure 8, there are two attenuators. One attenuator is a variable 127 dB attenuator and the other is a 3 dB attenuator. During the first part of the test, the variable attenuator is set to an initial level of 0 dB and the 3 dB attenuator is switched into the IF path. A voltage measurement is taken and then the 3 dB attenuator is switched out of the circuit and another voltage measurement is made. We add 4 dB more of attenuation using the variable attenuator and then switch the 3 dB attenuator into and out of the path as before. This process is repeated until we reach a final value of the variable attenuator, which in our case was 32 dB. The powers are calculated for each attenuator setting both with the 3 dB attenuator in and out, and from this a mean dB value is calculated, which is a ratio of the power with the 3 dB attenuator out to that with the 3 dB attenuator in. A low power mean is determined and subtracted from the values calculated above. This power ratio is plotted in Figures 14 and 15 versus output power with the 3 dB attenuator switched in. The IF system is considered linear when the ratio of these powers is constant to within 0.1 % or ± 0.005 dB. In Figures 14 and 15, the solid black lines are our quoted uncertainties. For output powers between 0.02 and 10 mW our measurements are well within these uncertainties. The variable attenuator is typically set at 6 dB for these measurements. At this setting, the cryogenic standard's output power ranges from 0.1 to 0.3 mW across the frequency band. Our hottest check standard has an output power of approximately 5 to 7 mW at this attenuator setting. Also, the IF is checked for every measurement, as described in Section 3.6.

The final linearity measurements tested the linearity of the entire system. These measurements test the linearity of the RF amplifier at the front end of the radiometer path as well as everything behind this amplifier. Two check standards are measured and their noise temperatures are recorded. For this test we measured two different check standards on two separate ports. A 3-dB attenuator is then inserted between the switch port and one of the check standards. Each standard was measured 10 times and then the attenuator was taken out of the path and another 10 measurements were made. We want to ensure that the noise temperature of the check standard is the same in either case. Both standards were measured on ports 3 through 6 of the switch head, but results for only two of the ports will be shown. Check standard X12ZHZ.411 measured on port 5 is shown in Figure 16 and check standard X12ZHZ.565 measured on port 6 is shown in Figure 17. The largest difference between any two measurements is 47 K shown in Figure 16 at 11 GHz. The uncertainty in the attenuator characterization can induce an uncertainty of approximately 70 K in the measurements with the attenuator and therefore this 47 K difference in the measurements is acceptable. The sample standard deviation for the 10 measurements was between 10 K to 20 K.
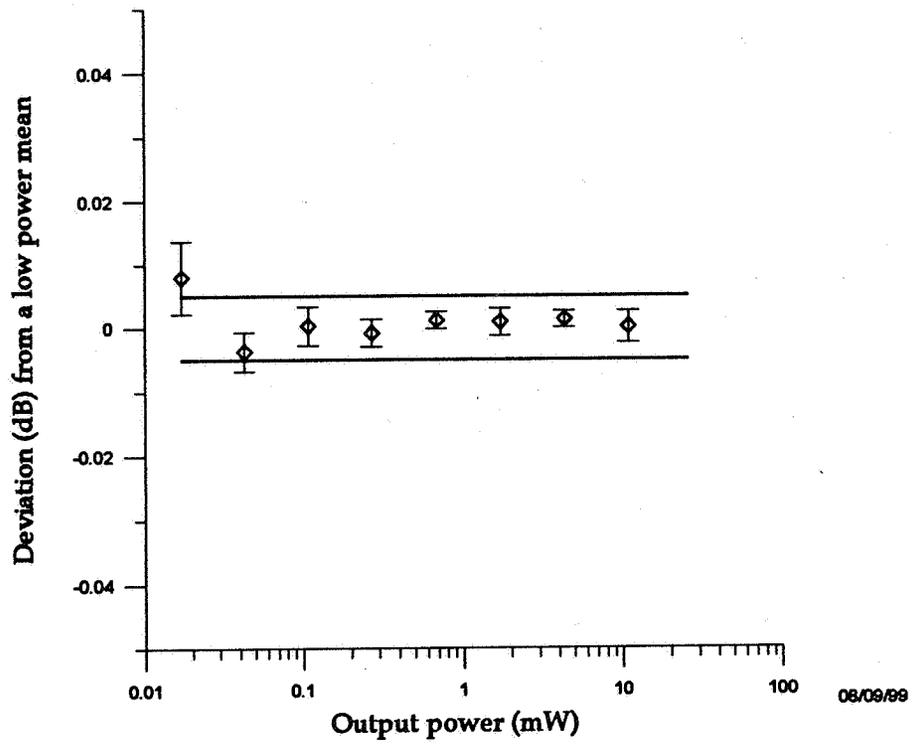
18

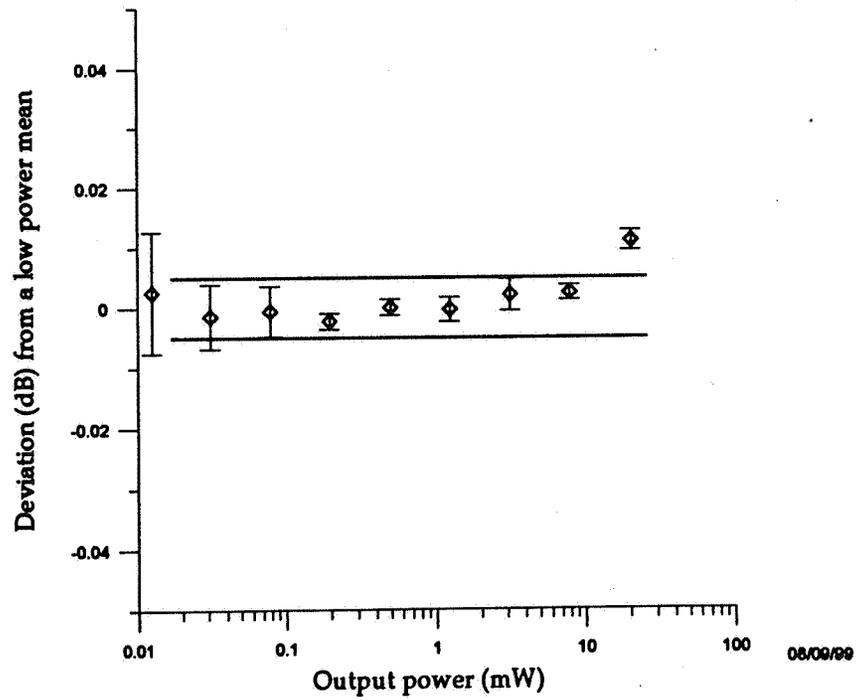Figure 14. IF linearity test at 8 GHz.

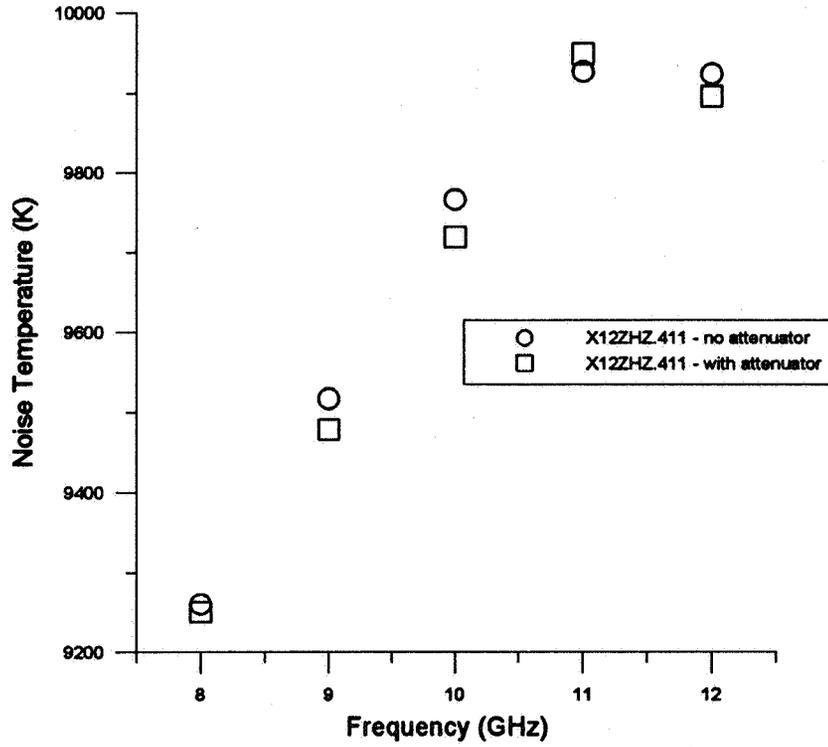Figure 15. IF linearity test at 12 GHz.

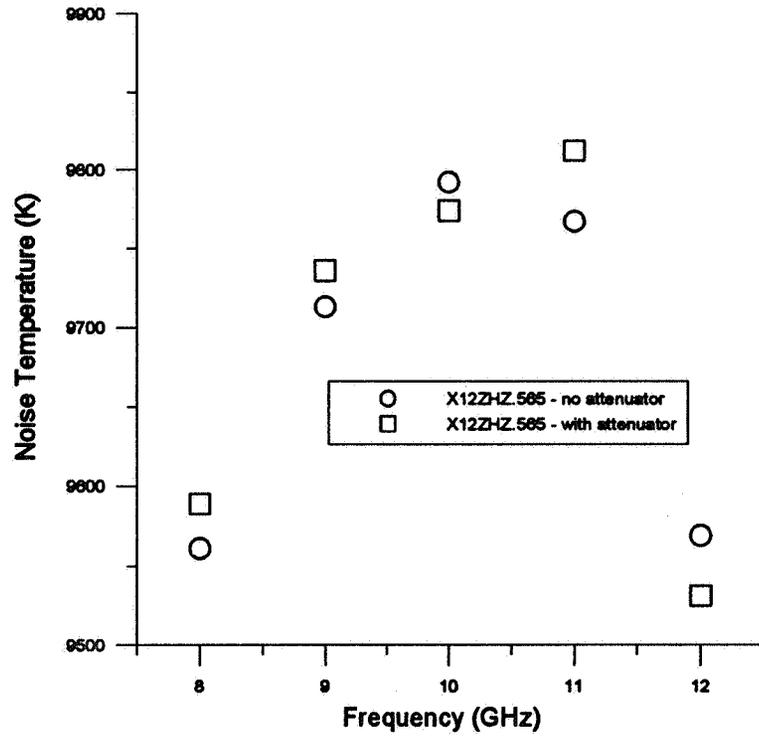Figure 16. RF linearity test - check standard X12ZHZ.411.

Figure 17. RF linearity test - check standard X12ZHZ.565.

4.7 Spurious signals

We test for harmonic interference or spurious signals that could be present in the power measurements. We check that lower frequencies are not generating harmonics in the frequency band of interest and that frequencies in the measurement band are not generating higher harmonics both within the measurement band and outside this band. The filters, mixer, and amplifiers are designed to minimize this possibility. The RF amplifier is designed to amplify only in the frequency band of interest. The low-pass filters are designed to pass everything below the upper end of the band we are interested in. The mixer is band-limited, double balanced, and designed to eliminate the second harmonic within the same band and anything outside of the frequency band of interest. For the 8 to12 GHz system, we have to worry about the harmonics that generate signals inside this frequency band. The way this was tested is as follows: An 8 GHz low-pass filter was inserted between the port and the DUT. This eliminates frequencies above 8 GHz, thereby eliminating the true signal. In the absence of the true signal, the measured noise temperature should equal the ambient temperature, 296 K. If any of the above mentioned frequencies were getting through, they would appear as a deviation from ambient temperature above 8 GHz. The results of this test are shown in Figure 18. We see that at 8 GHz, the signal does get through the filter but is eliminated at 9, 10, 11, and 12 GHz. This shows that spurious signals are not present at a measurable level.

4.8 Mismatch Factors/Asymmetry

The mismatch factors and asymmetry are used in the calculation of noise temperature. The mismatch factor is the ratio of delivered power to available power across an interface. Asymmetry is a ratio of the efficiency in one path compared to the efficiency in another path. The efficiency is defined as the ratio of the power delivered at one interface to the power delivered at another interface. In effect, it is a measure of the path loss. In previous systems, the mismatch and efficiency were measured using six-port measurements [1, 2]. In the present system, the mismatch factors are calculated from measured reflection coefficients as shown in eq (6), and the efficiencies for each port are measured directly on the VNA [6]. The asymmetry is just the ratio of the efficiency of the cryogenic port to the efficiency of the DUT port.

To ensure that the mismatch factor was computed correctly we made sure it was similar in magnitude to previous mismatches and also checked the program computations manually. During the initial stages of development, the efficiency was computed using the following equation,

$$\eta = \frac{|S_{21}|^2(1-|\Gamma_{rad}|^2)}{|1-S_{22}\Gamma_{rad}|^2 - |(S_{12}S_{21} - S_{11}S_{22})\Gamma_{rad} + S_{11}|^2} , \qquad (11)$$

where the S-parameters are the measured S-parameters of the switch and Γ_{rad} is the reflection coefficient of the radiometer. Initially, we planned to cascade the S-parameters of the switch and the necessary reflection coefficients for both the efficiencies and the mismatches. We found that we could not get repeatability between measurements because the uncertainty in the individual
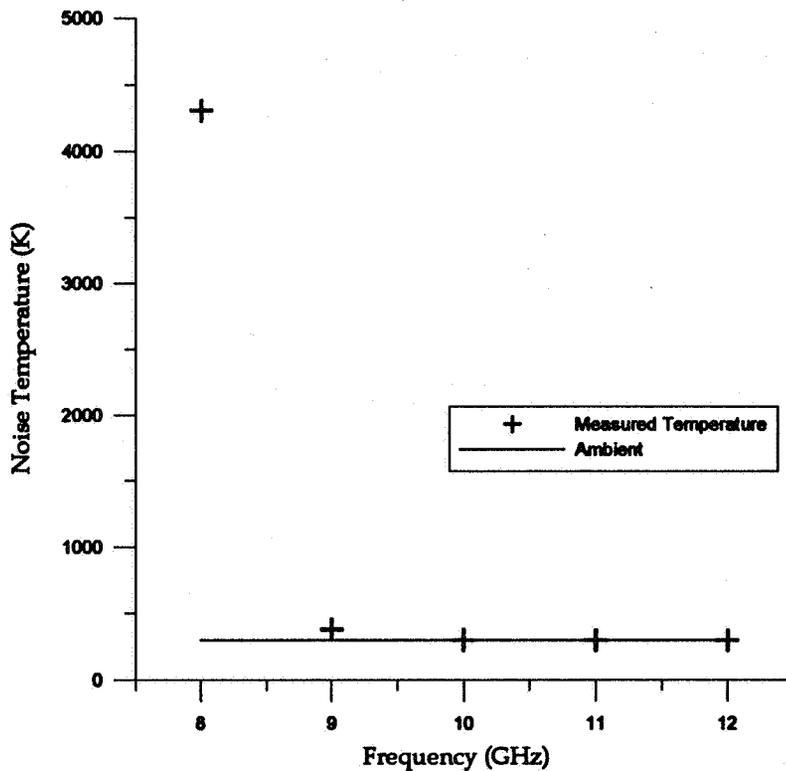
21

Figure 18. Measurement of spurious signals.

measurements was too large. We therefore decided to measure the reflection coefficient looking into the combination of the switch and the radiometer together for the mismatches and measure the efficiency directly, as mentioned above. At this point we were able to repeat measurements between ports and the RF linearity test succeeded.

Figure 19 shows the comparison between measuring the efficiency using a one-port adaptor characterization technique [6], and using a Transmission-Reflection-Line (TRL) calibration to measure the S-parameters and convert these into an efficiency. We use one-port technique because the measurement is easier and because, during a calibration, the cables do not have to be moved.

4.9 Repeatability and Time Dependence of Reflection Coefficients

As previously stated, the six-port measurements of reflection coefficients have been eliminated in the new system. Since the reflection coefficients are no longer measured for each noise-temperature measurement, change over small time scales will be unaccounted for in the new system. It is therefore imperative that we check the repeatability and time dependence of the reflection coefficients measured on the VNA.

We plan to measure the reflection coefficients of the check standards and radiometer plus
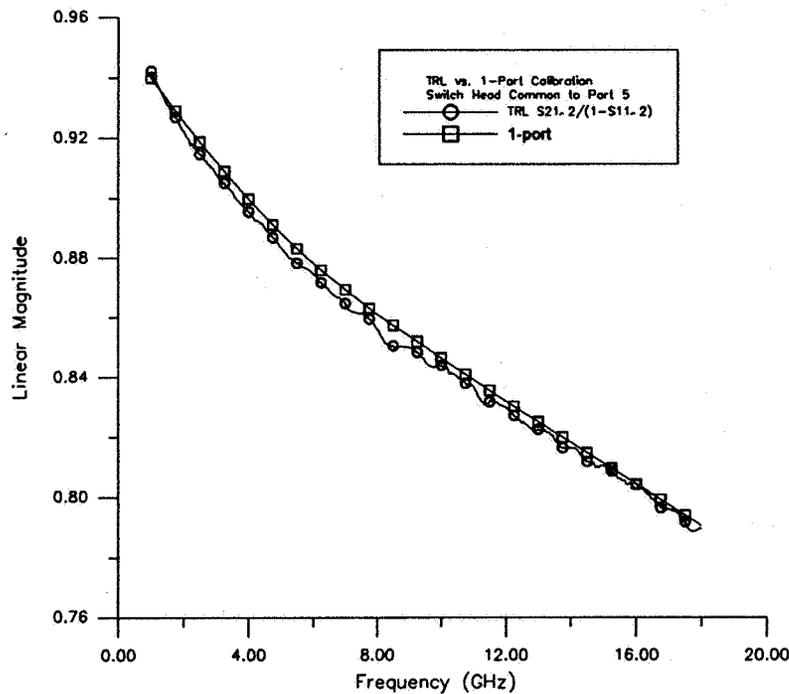
22

Figure 19. Comparison between two-port measurement of
efficiency and a one-port measurement.

switch head path efficiencies every 6 months. The radiometer plus switch head combination was
measured in May, 1999 and again in November, 1999. Results for ports 2 and 5 are shown in
Figures 20 and 21. These results show that the repeatability in efficiency is within 0.002 for
average maximum deviations for port 2 shown in Figure 20 and 0.003 for port 5 shown in Figure
21. The calculated uncertainty in efficiency from 2 to 12.4 GHz is 0.0034, so that the repeatability
of the measurements is within this uncertainty. The repeatability of these measurements is strongly
dependent on the repeatability of VNA calibrations.

4.10 Comparison

As a final check of the entire new system, we can compare the noise temperatures
measured on the new system to those measured by the older coaxial system. The results of this
test are shown in Figures 22 and 23. The NFRad measurement shown is an average value for 12
independent measurements on different ports. The historical measurement shown is an average
value for all measurements taken on the old coaxial system. No measurements were ever taken at
10 or 11 GHz on the older system and the 7 mm check standards. For both sets of data, the error
bars correspond to expanded (k = 2), combined (dominantly type-B) uncertainties, excluding the
cryogenic standard uncertainty, which would be common to both. The average noise temperatures
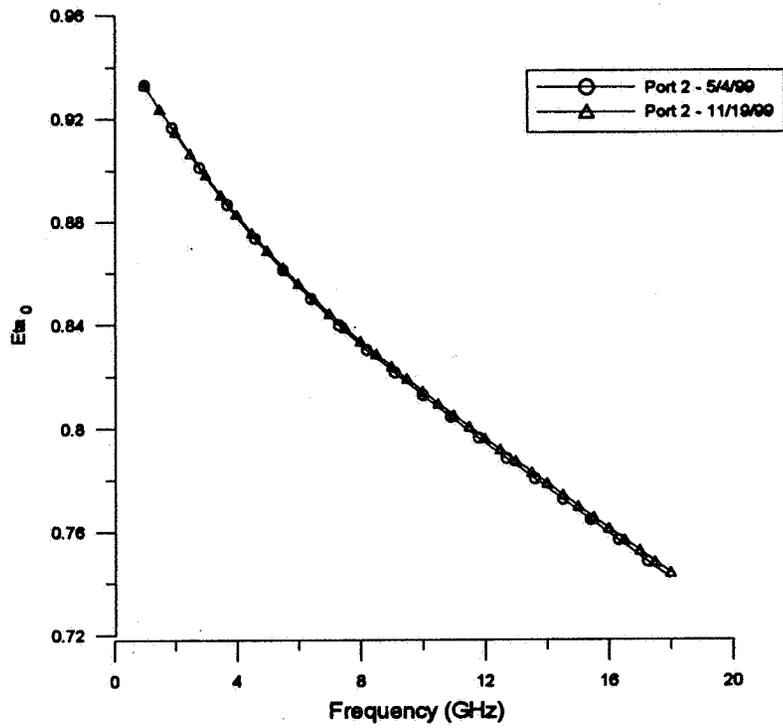between the two systems agree to within 45 K, which is well within estimated uncertainties.

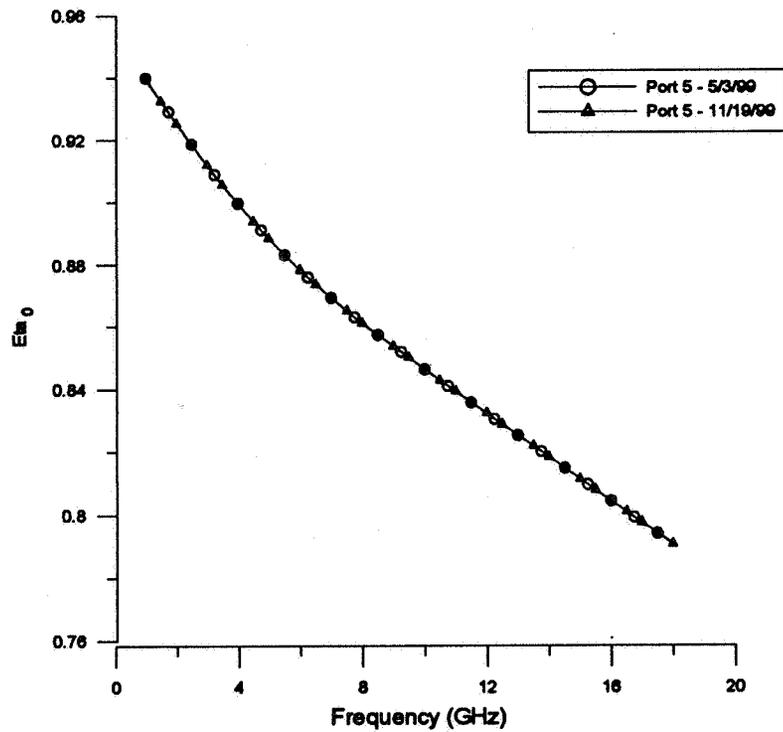Figure 20. Time dependence of efficiency measurements on port 2.

Figure 21. Time dependence of efficiency measurements on port 5.

5. UNCERTAINTY ANALYSIS

5.1 Background

The uncertainty analysis closely follows that for the other NIST total-power radiometers [8]. In keeping with the notation of references [9] and [10], we will use u_{T_x} to denote the standard uncertainty in the measurement of T_x. The combined standard uncertainty is composed of type-A and type-B uncertainties. Type-A uncertainties are those that are measured and determined by statistical methods, typically the standard deviation of the mean of several independent measurements of the quantity of interest. Type-B uncertainties are those determined by other means, such as estimates of systematic uncertainties. We shall deal primarily with type-B uncertainties; the type-A uncertainty is treated near the end of this section. We use $\mathscr{E}$ to denote the fractional standard uncertainty in a parameter; for example, $\mathscr{E}_{cry} = u_{TCry}/T_{cry}$. The contribution of the uncertainty in a particular parameter (e.g., T_{Cry}) to the uncertainty in T_x will be denoted $u_{T_x}(\text{Cry})$.

The noise temperature of a device being measured is determined by the radiometer equation, eq (5). Uncertainties in T_x arise due to uncertainties in the determination of the quantities appearing on the right side of eq (5) and due to departures from perfect isolation and linearity, which were assumed in deriving the radiometer equation. For quantities appearing in eq (5), the propagation of uncertainties is treated in the usual manner, outlined in reference [8]. Reference [8] treated the following contributions to the uncertainty in T_x : the cryogenic standard, the ambient standard, the mismatch factors, the asymmetries, radiometer isolation, broadband mismatch effects, nonlinearity effects, the power ratio measurements, and connector repeatability.
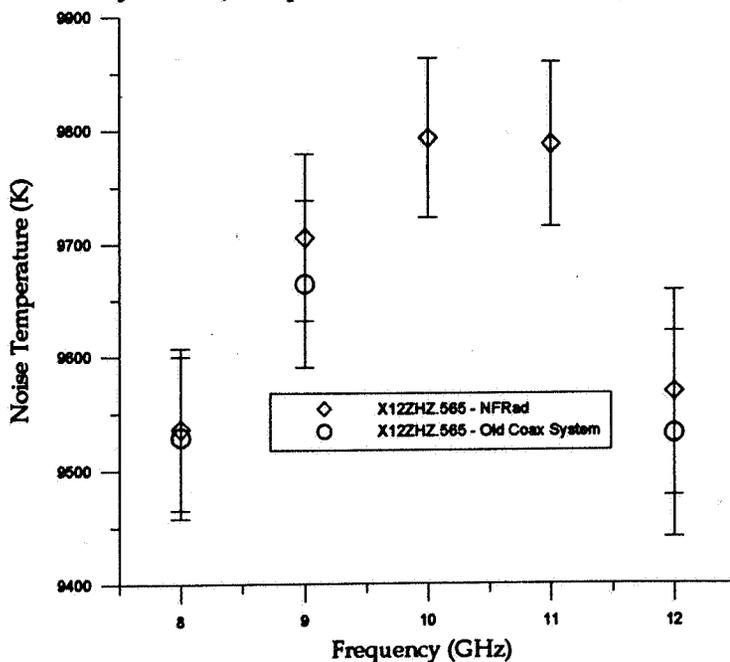

Figure 22. Measurement comparison between old coax system and NFRad for X12ZHZ.565.
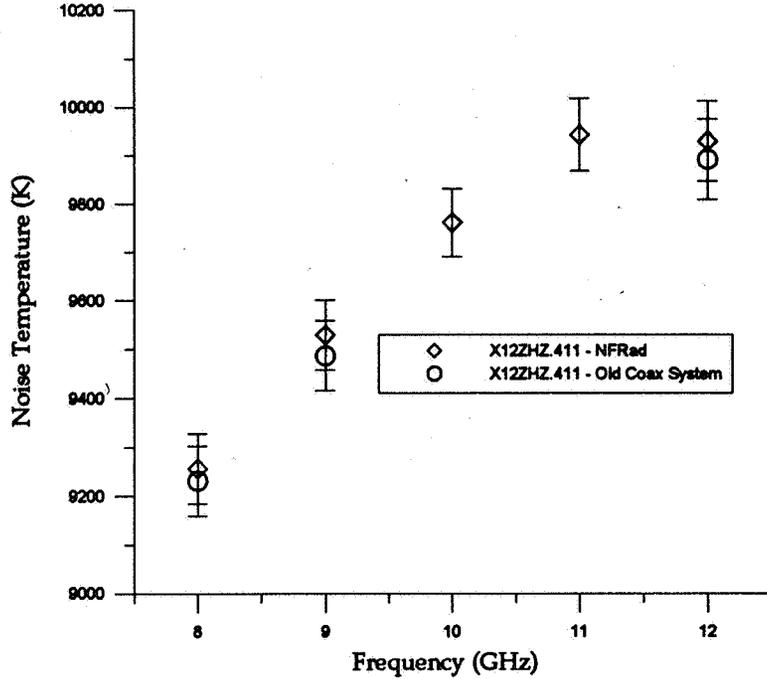
Figure 23. Measurement comparison between old coax
system and NFRad for X12ZHZ.411

We shall deal with each in the following subsections.

5.2 Primary Standards

The cryogenic standard contributes to the uncertainty in T_x as

$$\frac{u_{T_x}(Cry)}{T_x} = \left|1 - \frac{T_a}{T_x}\right|\left|\frac{T_s}{T_a - T_s}\right| \mathscr{E}_{Cry}. \tag{12}$$

The cryogenic standard that will be used with this radiometer will typically be Standard C, a coaxial standard with a GPC-7 connector. Its fractional uncertainty is given by reference [8]

$$\mathscr{E}_{Cry} = \left[1.813 + 0.02284f + 0.16A(f)^2\right]^{1/2}/\sqrt{3},$$

$$A(f) = 0.0283\sqrt{f} + \frac{0.0660}{1 + \frac{0.3654}{f^2}}. \tag{13}$$

This yields a fractional uncertainty of around 0.8 % over the frequency range of operation of Standard C (1 to 12 GHz), which corresponds to an uncertainty of about 0.3 % in T_x for a typical

26

hot (9000 K) noise source.

The contribution of the uncertainty in the ambient standard temperature to the uncertainty in the DUT noise temperature is given by

$$\frac{u_{T_x}(amb)}{T_x} = \left| \frac{T_x - T_s}{T_a - T_s} \right| \frac{T_a}{T_x} \mathscr{E}_{T_a}. \tag{14}$$

The design of the ambient standard is discussed above. Its physical temperature is measured with a calibrated thermistor. A conservative estimate of the uncertainty in the temperature measurement is $u_{T_a} = 0.1$ K or $\mathscr{E}_{T_a} = 0.034$ %.

5.3 Mismatch Factors

The ratio of mismatch factors contributes to the uncertainty in the DUT noise temperature according to,

$$\frac{u_{T_x}(M/M)}{T_x} = \left| 1 - \frac{T_a}{T_x} \right| \mathscr{E}_{M/M} \approx \left| 1 - \frac{T_a}{T_x} \right| u_{M/M}. \tag{15}$$

The mismatch uncertainty depends strongly on the poorly known correlation between uncertainties in the measurements of different reflection coefficients and again [8] we will use the maximum of the uncertainties obtained by assuming complete correlation and no correlation whatsoever,

$$u_{M/M} = Max\left(u_{cor}, u_{uncor} \right). \tag{16}$$

The correlated and uncorrelated uncertainties are given by [8],

$$u_{M/M}(cor.) = 4 u_{Im\Gamma} \left| y_S + y_{r,S} - y_x - y_{r,x} \right|,$$

$$u_{M/M}(uncor.) = 2\sqrt{2}\, u_{Re\Gamma} \left[(x_S - x_{r,S})^2 + (y_S + y_{r,S})^2 + (x_x - x_{r,x})^2 + (y_x + y_{r,x})^2 \right]^{1/2}, \tag{17}$$

where x and y refer to real and imaginary parts of the corresponding reflection coefficients. What remains is to estimate $u_{Re\Gamma}$ and $u_{Im\Gamma}$. In NFRad the reflection coefficients are measured with a commercial VNA, unlike the previous generation of NIST radiometers, which used internal six-port reflectometers. The VNA manufacturer's specifications for measurements of small reflection coefficients are an uncertainty in $|\Gamma|$ of about 0.0007 between 2 GHz and 18 GHz. We find this number to be uncomfortably small and choose instead to continue using

$$u_{Re\Gamma} = u_{Im\Gamma} = 0.0025, \tag{18}$$

27

as in the old radiometers. This value is also large enough to include any change in the reflection coefficients of the radiometer or standard since the time of their measurement. (We no longer measure at the time of the noise-temperature measurement, but rather look up previously measured values.) Our experience, reinforced by the test of Subsection 4.8 above, is that changes in the reflection coefficients over time are normally smaller than the repeatability limits of such measurements.

5.4 Asymmetry

The asymmetry is defined as the ratio of efficiencies η_a/η_x appearing in the radiometer equation. Its contribution to the uncertainty in the measured noise temperature is

$$\frac{u_{T_x}(\eta/\eta)}{T_x} = \left|1 - \frac{T_a}{T_x}\right| u_{\eta/\eta}, \tag{19}$$

where we have used $\mathscr{E}_{\eta/\eta} \approx u_{\eta/\eta}$. With NFRad, there are three different methods which could be used to evaluate the asymmetry. It is still possible to use what is called the "manual asymmetry method," which is used in the old coaxial and waveguide radiometers. The fractional uncertainty in the asymmetry using this method is given by [8] $u_{\eta/\eta} = 0.8 u_{R_a\Gamma}$, which from eq (8) is $u_{\eta/\eta} = 0.002$. (Equations (23, 56, 57) in reference [8] are missing a factor of 2.)

The second method to determine the asymmetry is called the S-parameter method. It uses the measured S-parameters of the switch head to compute the relevant efficiencies directly and takes the ratio to obtain the asymmetry. The uncertainty in this method is dominated by the uncertainty in measuring $|S_{21}|^2$ for each path. Using the VNA manufacturer's specifications for this uncertainty we get $u_{\eta/\eta} = 0.0044$ for the asymmetry between 2 GHz and 18 GHz. In practice, our uncertainty will be somewhat larger than this value because in the actual measurements on the switch, there is some bending of the cables required by the fact that the switch ports being measured are generally not directly across from each other.

The third method for measuring the asymmetry is to measure the two efficiencies directly, using the reflective termination (RT) method developed by Daywitt [6, 7]. This method computes the intrinsic efficiency of a passive two-port from the reflection coefficients measured when one of the ports is terminated in two different reflective terminations. The uncertainty analysis for this method was presented in references [8] and [11]. That same analysis applied to the measurements made on the various switch paths (common to ports 3 through 6) resulted in uncertainties in the ratio of efficiencies of 0.0047 from 1 GHz to 2 GHz, 0.0034 from 2 GHz to 12.4 GHz, and 0.0047 from 12.4 GHz to 18 GHz.

The manual asymmetry method is therefore the most accurate way to measure the asymmetry, with a contribution to the fractional uncertainty in T_x of about 0.2 %. However, it is relatively slow compared to the other methods, and it not suited to swept measurements. Thus it is

28

not practical to use the manual asymmetry method for all the frequencies (every 0.05 GHz) stored in the system table. We choose to use the reflective termination technique initially, leaving open the possibility of using the manual asymmetry method if smaller uncertainties are desired at selected frequencies.

5.5 Other Type-B Uncertainties

Previous uncertainty analyses for NIST radiometers [1,8] included an explicit "connector" contribution. Connector variability arises from differences between repeated connections of the same pair of connectors and from differences between different pairs of connectors, such as the difference between the DUT-VNA connection and the DUT-radiometer connection. For the most part, connector variability is included in $u_{Re\Gamma}$ in the mismatch and asymmetry uncertainties. It is also included (roughly) in the type-A uncertainty computed from multiple measurements with the sources disconnected between measurements. The connector uncertainty included previously accounted for the possibility of a connector composed of a different metal with significantly different properties. We consider this an unlikely prospect now for coaxial connectors below 18 GHz, and choose to merely exclude this case from the range of applicability of the analysis. Even the case of different metals is less important for NFRad because the VNA measurements in GPC-7 define the reference plane at the center of the connection, so that the reflection coefficient of a device carries with it information about its connector. This was not so in the previous generation of NIST radiometers, which defined the reference plane with the entire connection included in the radiometer. We conclude that the variability in the connector is adequately accounted for in the mismatch and asymmetry uncertainties, and do not include a separate connector contribution to the uncertainty in T_x.

The measured powers enter the radiometer equation through the ratios $Y_x \equiv p_x/p_a$ and $Y_s \equiv p_s/p_a$ in the factor $Y = (Y_x - 1)/(Y_s - 1)$. The powers are measured in the same manner in NFRad as in the previous NIST systems, and the uncertainty is the same as well,

$$\frac{u_{T_x}(Y)}{T_x} \le \left|1 - \frac{T_a}{T_x}\right| \times 0.04\,\% . \tag{20}$$

This is negligible unless $T_a \ge 3\,T_x$.

The uncertainty due to imperfect isolation was given in [8] for 40 dB, 45 dB, and 50 dB isolation. The 8 to 12 GHz radiometer for NFRad has 60 dB of isolation across its bandwidth. In this case the uncertainty due to imperfect isolation is given by

$$\frac{u_{T_x}(isol)}{T_x} = 0.01 \times \left[0.08\,|\Gamma_s|\left|1 - \frac{T_a}{T_x}\right| + 0.008\left|1 - \frac{T_s}{T_x}\right| + 17\frac{|\Gamma_x|}{T_x}\right], \tag{21}$$

which is typically negligible.

The uncertainty due to frequency offset and broadband mismatch is of the same form as in reference [8],

$$\frac{u_{T_x}(BBMM)}{T_x} = \frac{200\%}{\sqrt{3}} \left| \cos\left(\frac{4\pi f_{IF} l}{30}\right) sinc\left(\frac{\pi B l}{15}\right) - 1 \right| \times (|\Gamma_x \Gamma_{r,s}| + |\Gamma_x \Gamma_{r,x}|) \left| 1 - \frac{T_a}{T_x} \right|, \quad (22)$$

where f_{IF} is 0 for NFRad, $B = 0.010$ is the bandwidth in GHz, and $l= 42.3$ is the physical length in centimeters from the input port to the beginning of the first isolator in the radiometer. As was done for other NIST radiometers, NFRad was designed so that the broadband mismatch uncertainty is negligible.

The linearity of the IF section is checked the same way it was with the old system. For each noise temperature measurement, twenty five readings are taken with a 3 dB attenuator switched in the IF section of the system, and twenty five readings are taken without the attenuator. The two resulting noise temperatures must agree to within 0.2 %. This is taken to be the maximum or expanded ($k = 2$) uncertainty, leading to a standard uncertainty of

$$\frac{u_{T_x}(lin)}{T_x} = 0.10 \%. \quad (23)$$

5.6 Type-A Uncertainty

In noise-temperature calibrations using NFRad, we repeat measurements on two different levels. Typically, we do three separate measurements of the noise temperature, one on each of three different ports. For each of these separate measurements we do 50 readings (25 each with and without the 3 dB attenuator in the IF section) of the delivered powers from the two standards and from the DUT. A noise temperature of the DUT is computed for each DUT power reading. Thus in a typical calibration, we have three separate measurements times 50 readings, for a total of 150 values of the noise temperature, which are combined to obtain the final value for the measured DUT noise temperature. The question of how to evaluate the type-A uncertainty in obtaining the average value from the multiple measurements was addressed in Section 3.10 of reference [8] for a more complicated measurement scheme. We follow that treatment here, simplifying as appropriate.

We use T_{ij} for the value of a single reading of the noise temperature. The index i, which denotes the number of the measurement, runs from 1 to N_M (typically 3); the index j, denotes the reading number and runs from 1 to N_R (typically 50). We assume that the number of readings N_R is the same for each measurement. We use T_i to denote the mean of the N_R readings for each measurement and use σ_i for the associated standard deviation,

30

$$T_i = \frac{1}{N_R} \sum_{j=1}^{N_R} T_{ij},$$

$$\sigma_i^2 = \frac{1}{(N_R - 1)} \sum_{j=1}^{N_R} (T_i - T_{ij})^2,$$

(24)

and we use T and σ for the mean and standard deviation of the N_M measurements,

$$T = \frac{1}{N_M} \sum_{i=1}^{N_M} T_i,$$

$$\sigma^2 = \frac{1}{(N_M - 1)} \sum_{i=1}^{N_M} (T_i - T)^2.$$

(25)

To develop the general expression for u_A we model [12] the variable T_{ij} as

$$T_{ij} = \tau + M_i + R_{ij},$$

(26)

where τ is the true value for the noise temperature of the device being measured, M_i is a random variable representing variations from measurement to measurement (i), and R_{ij} is a random variable that varies with the reading j and the measurement i. Our estimate of the true value is just the mean of all the readings,

$$\tau \approx T \equiv \frac{1}{N_M N_R} \sum_{i=1}^{N_M} \sum_{j=1}^{N_R} T_{ij},$$

(27)

which is also equal to the mean of the N_M separate measurements. The means of the two random variables are both zero, and their variances will be denoted by

$$\langle M_i^2 \rangle = v_M,$$

$$\langle R_{ij}^2 \rangle = v_R,$$

(28)

where the averages are over all indices. The variances can be estimated from the measured values T_{ij} by

31

$$\frac{1}{N_M(N_R - 1)} \sum_{i,j} (T_{ij} - T_i)^2 \approx v_R,$$

$$\frac{1}{(N_M - 1)} \sum_i (T_i - T)^2 \approx v_M + \frac{v_R}{N_R}.$$

(29)

The equalities are only approximate because we are dealing with a limited sample. We can solve eq (29) for v_R and v_M, and use eqs (24) and (25) to write

$$v_R = \langle \sigma_i^2 \rangle,$$

$$v_M = \sigma^2 - \frac{v_R}{N_R},$$

(30)

where the averages are over all free indices and where it is understood that if a negative value results for v_M it is taken to be 0. The type-A uncertainty in the determination of $\tau \approx T$ is then the square root of the variance in T,

$$u_A \approx \sqrt{\frac{v_M}{N_M} + \frac{v_R}{N_M N_R}}.$$

(31)

Comparison to eq (30) reveals that eq (31) is equivalent to $u_A^2 = \sigma^2 / N_M$, provided that eq (30) does not result in a negative value for v_M. This is as it should be: if we did enough independent measurements to determine σ^2 well, that would be sufficient, since it includes the variations from one reading to another. Since we only do three separate measurements, we supplement that information with the measured σ_i^2.

5.7 Combined Uncertainty

The type-B standard uncertainty for a single noise temperature measurement is obtained by forming the square root of the sum of the squares of the individual contributions eqs (12, 14, 15, 19, 20, 21, 22, 23),

$$u_B = [u_{T_x}^2(Cry) + u_{T_x}^2(amb) + u_{T_x}^2(Y) + u_{T_x}^2(M/M) + u_{T_x}^2(\eta/\eta)$$

$$+ u_{T_x}^2(isol) + u_{T_x}^2(BBMM) + u_{T_x}^2(lin)]^{\frac{1}{2}}.$$

(32)

In calibrating a customer's device, we make several measurements of its noise temperature.

32

Because the uncertainty defined by eq (32) depends on the measured noise temperature and on various measured reflection coefficients, it is in principle different for each of the separate measurements of the device's noise temperature. In practice, however, there is little difference between the values, and we use the maximum.

The expanded (k = 2) combined uncertainty is computed from eqs (31) and (32),

$$U_{T_x} = 2\sqrt{u_A^2 + u_B^2}.$$ (33)

The expanded uncertainty varies with the device being tested, the frequency, and the method of measuring the asymmetry. Assuming the reflective termination method is used to measure the asymmetry, a typical value for a GPC-7 source with high noise temperature (above a few thousand kelvins) would be about 1 %. Sources with other coaxial connectors would be measured through adaptors, and the uncertainty would be somewhat larger. If the asymmetry were measured with the manual method, the uncertainty would be somewhat smaller.

6. SUMMARY

The NIST Noise Project has recently completed design, construction, and testing of a new noise temperature/figure measurement system with an 8 to 12 GHz radiometer for a GPC-7 coaxial environment. This note described the design and testing of the system, the operation of the system and an outline of the measurement procedures. A discussion of the various tests used to verify the system and the uncertainty analysis were also presented. The measurements on this system can be obtained more quickly and the system is easier to use than previous coaxial systems. Another advantage is that the system is less temperamental, due to the absence of the six-port reflectometer, than previous systems. This system is also suitable for noise parameter measurements.

---

7. REFERENCES

[1]   Daywitt, W.C. Radiometer equation and analysis of systematic errors for the NIST automated radiometers. Natl. Inst. Stand. Technol. Tech. Note 1327; 1989 March.

[2]   Randa, J.R.; Terrell, L.A. Noise temperature measurement system for the WR-28 band. Natl. Inst. Stand. Technol. Tech. Note 1395; 1997 August.

[3]   Pucic, S.P. Measurement of noise—An introduction. IEEE MTT-S International

Microwave Symposium: Workshop, 1994 May.

[4]   Daywitt, W.C. A coaxial noise standard for the 1 GHz to 12.4 GHz frequency range.
        Natl. Inst. Stand. Technol. Tech. Note 1074; 1984 March.

[5]   Larsen, N.T. A new self-balancing DC-substitution RF power meter. IEEE Trans. IM-
        25(4): 343-347; 1976 December.

[6]   Daywitt, W.C. Determining adaptor efficiency by envelope averaging swept frequency
        reflection data. IEEE Trans. MTT-38(11): 1748-1752; 1990 November.

[7]   Pucic, S.P., Daywitt, W.C. Single-port technique for adapter efficiency evaluation. 45th
        ARFTG Conference Digest, Orlando, FL, pp. 113-118; 1995 May.

[8]   Randa, J. Uncertainties in NIST noise-temperature measurements. Natl. Inst. Stand.
        Technol. Tech. Note 1502; 1998 March.

[9]   ISO Guide to the Expression of Uncertainty in Measurement. International Organization
        for Standardization; Geneva, Switzerland; 1993.

[10]   Taylor, B.N.; Kuyatt, C.E. Guidelines for evaluating and expressing the uncertainty of
        NIST measurement results. Natl. Inst. Stand. Technol. Tech. Note 1297, 1994 edition;
        1994 September.

[11]   Randa, J.; Wiatr, W., and Billinger, R.L. Comparison of adapter characterization methods.
        IEEE Trans. MTT-47(12): 2613-2620; 1999 December.

[12]   Graybill, F.A. Theory and Application of the Linear Model. Duxbury Press; Belmont, CA;
        1976.